Atomic Spectroscopy

Article

A Quantity Chalcopyrite Reference Material for In Situ Sulfur Isotope Analysis

Youwei Chen,[a,*] Liemeng Chen,[a] Guoqiang Tang,[b] Zhian Bao,[c] Zexian Cui,[d] Xincheng Qiu,[e] Zhong-Qiang Chen,[e] Jing Gu,[a] Shaohua Dong,[a] and Jianfeng Gao[a,*]

[a] State Key Laboratory of Ore Deposit Geochemistry, Institute of Geochemistry, Chinese Academy of Sciences, Guiyang 550081, China

[b] State Key Laboratory of Earth and Planetary Physics, Institute of Geology and Geophysics, Chinese Academy of Sciences, Beijing 100029, China

[c] State Key Laboratory of Continental Dynamics, Department of Geology, Northwest University, Xi'an 710069, China

[d] State Key Laboratory of Isotope Geochemistry, Guangzhou Institute of Geochemistry, Chinese Academy of Sciences, Guangzhou 510604, China

[e] State Key Laboratory of Biogeology and Environmental Geology, China University of Geosciences, Wuhan 430074, China

Received: *June 25, 2023;* ***Revised:*** *July 19, 2023;* ***Accepted:*** *July 24, 2023;* ***Available online:*** *July 26, 2023.*

DOI: 10.46770/AS.2023.141

ABSTRACT: Secondary ion mass spectrometry (SIMS) for sulfur isotope analysis in chalcopyrite is an essential technique with exceptional spatial resolution, which enables precise constraints on mineralization mechanisms. However, the scarcity of matrix-matched chalcopyrite reference materials (RM) for SIMS hinders its accuracy and reliability. This study introduces a large-grained natural chalcopyrite RM (IGSD) for precise sulfur isotope analysis ($\delta^{34}S$) using SIMS and laser ablation multicollector-inductively coupled plasma mass spectrometry (LA-MC-ICPMS). Petrographic examination and electron microprobe analysis (EMPA) results confirm the homogeneity of major elements in the IGSD chalcopyrite grains. The results of in situ analysis at four SIMS laboratories and one LA-MC-ICPMS laboratory and bulk analysis confirm the homogeneity of the S isotope composition in the IGSD chalcopyrite grains. The in situ analysis result is consistent with the result of isotope ratio mass spectroscopy (IRMS), which falls within the same range of uncertainty. This supports the suitability of the IGSD chalcopyrite RM for in situ S isotope analysis. The recommended $\delta^{34}S$ value of the IGSD chalcopyrite RM, based on IRMS, is 4.21 ± 0.23‰ (2SD, n = 30).

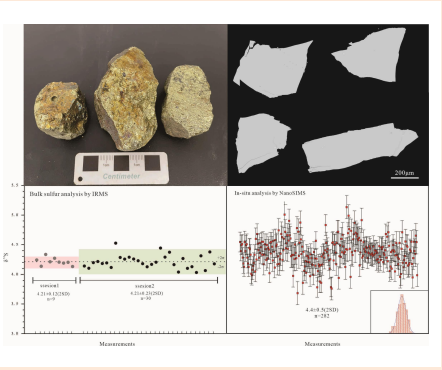

INTRODUCTION

Sulfur is widely distributed throughout the lithosphere, biosphere, hydrosphere, and atmosphere. Because of its multiple valence states and large differences in relative atomic masses, sulfur isotopes exhibit significant fractionation. Therefore, the sulfur isotopic systems are a valuable for tracing sulfur sources and constraining various geochemical processes.[1-4]

In recent years, in situ microanalysis techniques, such as LA-ICP-MS and SIMS have been widely adopted for sulfur isotope analysis.[5-15] Compared to traditional bulk methods, *e.g.*, RIGS, TIMS, and MC-ICPMS, in situ microanalysis offers several advantages, including increased efficiency, convenience, and notably, superior spatial resolution down to the micrometre scale, all while maintaining high precision.

SIMS-based sulfur analysis is a versatile and widely used in situ technique. It is characterized by high sensitivity and extremely high spatial resolution (1–20 μm),[11-14,16,17] which has a unique advantage in analyzing minerals with complex intergrown, heterogeneous, or zoning isotopic compositions. Therefore, sulfur isotope analysis through SIMS has proven to be a powerful tool for obtaining precise measurements of sulfur isotopes in minerals. This has enabled researchers to address a wide array of geological problems with high precision (~ 0.2‰).[12,14,15,18-23] However, instrumental mass fractionation (IMF) is a significant restraint factor for SIMS-based isotopic ratio analysis. Because of IMF, a systematic difference exists between the instrumentally measured

Table 1. The published $\delta^{34}S$ values in different sulfides (in-house standards or reference materials) for in situ Sulfur isotope analysis

Sample name	Material	$\delta^{34}S$ value with 2SD ‰ (method)	In-situ method	Ref.
Pyrite				
GAV-18	Natural material	9.62 ± 0.27 (LA-MC)	LA-MC	Craddock *et al.*[32]
PPP-1	Natural material	5.3 ± 0.2 (IRMS)	LA-MC and SIMS	Gilbert *et al.*[33]
Py1	Natural material	−0.6 ± 0.6 (IRMS)	LA-MC	Molnár *et al.*[34]
Py2	Natural material	−0.4 ± 1 (IRMS)	LA-MC	Molnár *et al.*[34]
10^{th}-1	PSPT	5.33 ± 0.27 (IRMS)	LA-MC	Feng *et al.*[35]
PSPT-2	PSPT	32.48 ± 0.29 (SN-MC)	LA-MC	Bao *et al.*[8]
GBW07267	RPP	3.46 ± 0.18 (SN-MC)	LA-MC	Chen *et al.*[31]
PAS-Py	PAS	18.22 ± 0.07 (IRMS)	LA-MC	Feng *et al.*[36]
RPPY	RPP	3.66 ± 0.24 (IRMS)	LA-MC	Lv *et al.*[37]
Balmat	Natural material	15.1 ± 0.2 (IRMS)	SIMS	Crowe *et al.*[38]
Ruttan	Natural material	1.2 ± 0.1 (IRMS)	SIMS	Crowe *et al.*[38]
CAR 123	Natural material	1.4 ± 0.4 (Unknown)	SIMS	Mojzsis *et al.*[39]
UWPy-1	Natural material	16.39 ± 0.40 (IRMS)	SIMS	Kozdon *et al.*[12]
SPAIN	Natural material	−2.95 ± 0.56 (Unknown)	SIMS	Kitayama *et al.*[40]
Sonora	Natural material	1.61 ± 0.16 (IRMS)	SIMS	Farquhar *et al.*[41]
Py-1117	Natural material	0.3 ± 0.1 (IRMS)	SIMS	Zhang *et al.*[17]
CS01	Natural material	4.6 ± 0.1 (IRMS)	SIMS	Zhang *et al.*[17]
Sierra	Natural material	2.17 ± 0.28 (IRMS)	SIMS	LaFlamme *et al.*[14]
Chalcopyrite				
CPY-1	Natural material	−0.7 ± 1.0 (IRMS)	LA-MC	Molnár *et al.*[34]
PSPT-1	PSPT	−0.73 ± 0.09 (SN-MC)	LA-MC	Bao *et al.*[8]
YN411-m	Glass	0.37 ± 0.24 (SN-MC)	LA-MC	Chen *et al.*[42]
GC	Natural material	−0.63 ± 0.12 (IRMS)	LA-MC	Chen *et al.*[42]
CPy-1	Natural material	4.3 ± 0.2 (IRMS)	LA-MC	Chen *et al.*[42]
TC1725	Natural material	12.78 ± 0.16 (IRMS)	LA-MC	Bao *et al.*[43]
PAS-Cpy	PAS	10.58 ± 0.33 (IRMS)	LA-MC	Feng *et al.*[36]
GBW07268	RPP	−0.57 ± 0.24 (SN-MC)	LA-MC	Chen *et al.*[31]
Norilsk	Natural material	8.0 ± 0.2 (IRMS)	SIMS	Crowe *et al.*[38]
Trout Lake	Natural material	0.3 ± 0.2 (IRMS)	SIMS	Crowe *et al.*[38]
OPM	Natural material	2.29 ± 0.56 (Unknown)	SIMS	Kitayama *et al.*[40]
Nifty-b	Natural material	−3.58 ± 0.44 (IRMS)	SIMS	LaFlamme *et al.*[14]
HTS4-6	Natural material	0.63 ± 0.16 (IRMS)	SIMS	Li *et al.*[44]
CPY-1	Natural material	1.4 ± 0.4 (Unknown)	SIMS	Li *et al.*[44]
Sphalerite				
NBS 123	PPP	17.09 ± 0.19	LA-MC	Pribil *et al.*[45]
PSPT-3	PSPT	26.40 ± 0.21 (SN-MC)	LA-MC	Bao *et al.*[8]
PAS-GBW07270	PAS	−5.44 ± 0.18 (IRMS)	LA-MC	Nie *et al.*[46]
SPH-1	RPP	−7.13 ± 0.41 (IRMS)	LA-MC	Lv *et al.*[37]
Balmat	Natural material	14.3 ± 0.2 (IRMS)	SIMS	Crowe *et al.*[38]
Chisel	Natural material	1.5 ± 0.1 (IRMS)	SIMS	Crowe *et al.*[38]
BT-4	Natural material	15.42 ± 0.14 (IRMS)	SIMS	Kozdon *et al.*[12]
JC-14	Natural material	4.9 ± 0.1 (IRMS)	SIMS	Zhang *et al.*[17]
MY09-12	Natural material	3.1 ± 0.1 (IRMS)	SIMS	Zhang *et al.*[17]
Galena				
CBI-3	Natural material	28.4 ± 0.36 (SN-SN-MC)	LA-MC	Chen *et al.*[47]
RPP-Gn	RPP	−0.94 ± 0.36 (SN-MC)	LA-MC	Chen *et al.*[31]
NWU-GN	RPP	28.27 ± 0.17 (IRMS)	LA-MC	Lv *et al.*[37]
UWGal-1	Natural material	16.61 ± 0.16 (IRMS)	SIMS	Kozdon *et al.*[12]
Pyrrhotite				
Po-10	Natural material	6.0 ± 0.1	LA-MC	Gilbert *et al.*[33]
Polo	Natural material	5.6 ± 1.2 (IRMS)	LA-MC	Molnár *et al.*[34]
Anderson	Natural material	1.4 ± 0.2 (IRMS)	SIMS	Crowe *et al.*[38]
Enon	Natural material	0.90 ± 0.56 (unknow)	SIMS	Kitayama *et al.*[40]
Alexo	Natural material	5.23 ± 0.40 (IRMS)	SIMS	LaFlamme *et al.*[14]
YP136	Natural material	1.5 ± 0.1 (IRMS)	SIMS	Li *et al.*[48]
JC-Po	Natural material	0.06 ± 0.33 (IRMS)	SIMS	Chen *et al.*[49]
Pentlandite				
Norilsk	Natural material	7.9 ± 0.2 (IRMS)	SIMS	Crowe *et al.*[38]
KA8	Natural material	2.21 ± 0.56 (unknow)	SIMS SIMS	Kitayama *et al.*[40]
VMSo	Natural material	3.22 ± 0.51 (IRMS)	SIMS	LaFlamme *et al.*[14]
JC-Pn	Natural material	−0.09 ± 0.15 (IRMS)	SIMS	Chen *et al.*[49]
Arsenopyrite				
RPP-Apy	RPP	−1.05 ± 0.15 (SN-MC)	LA-MC	Chen *et al.*[31]
YJS-65	Natural material	−1 (IRMS)	SIMS	Xie *et al.*[50]

Note: RPP: Resin-preserved powders; PSPT: pressed sulfide powder tablets; PAS: plasma-activated sintering synthesized; LA-MC: LA-MC-ICPMS; SN-MC: SN-MC-ICPMS.

and real values, which is intrinsically restrained by the composition and crystallographic orientation of the material under specific instrumental conditions.[14, 24-26] This indicates that IMF is ubiquitous and cannot be entirely eliminated. Thus far, the only reliable means of correction for IMF has been the use of homogeneous matrix-matched standards.[12,27,28] Thus, well-characterized, matrix-matched RMs for SIMS calibration are crucial for obtaining accurate sulfur isotopes.[14,29] The in-house standards and reference materials of different sulfides for in situ sulfur isotope analysis were compiled in Table 1. There are many synthetic and natural RMs for most sulfides. However, as a high-resolution surface analysis method, operating under ultra-high vacuum conditions, SIMS places considerable demands on the surface morphology. Moreover, SIMS is also affected by the crystal orientation of analyte. [12,13,30] Therefore, synthetic standards (such as the resin-preserved powders or pressed powder pellet standards), which were used in LA-MC-ICPMS,[31] may not be suitable for SIMS. Thus, the optimal sulfur isotopic standards for SIMS are natural minerals with homogeneous isotopic compositions. However, these natural RMs are relatively rare and limited for most sulfide minerals (Table 1).

Chalcopyrite ($CuFeS_2$) is an important source of copper and a primary copper sulfide in various types of deposits from magmatic (Cu-Ni sulfide systems) to various hydrothermal systems.[51-57] Therefore, the characteristics of chalcopyrite sulfur isotope ($\delta^{34}S$) have been extensively exploited for tracing metal sources and constraining the mineralization mechanism.[14,22,23,58-66] There are many natural and synthetic chalcopyrite RMs for LA-MC-ICPMS, as listed in Table 1. However, natural chalcopyrite references for SIMS are rare. Only few RMs are reported as working RMs for chalcopyrite SIMS-based sulfur isotope microanalysis, such as Trout Lake and Norilsk,[38, 39] OPM,[40] CPY-1 and CPY-2 (in-house standards),[34, 44] Nifity-b,[14] and HST-4-6.[44] However, the limited quantities of these RMs hindered their widely share and abroad application. Moreover, all these standards are selected from samples obtained from hydrothermal systems, where chalcopyrite grains are usually small and always precipitate with other sulfides, such as pyrite, sphalerite, galena, and pyrrhotite. As it can be challenging to isolate chalcopyrite grains for analysis, this is a significant limitation for microanalysis. Additionally, the softness of chalcopyrite crystals can make it difficult to achieve a smooth surface during polishing, particularly for small standards. Thus, there is an urgent need for a large quantity, high purity, and adequate size of the chalcopyrite standard that can address these challenges.

In this study, we provided a pure and large-grained chalcopyrite standard (IGSD) for sulfur isotope analysis ($\delta^{34}S$) through SIMS and LA-MC-ICPMS. The chalcopyrite is less impure in other minerals (only a few pyrrhotite or pentlandite grains are observed) owing to the origin of the high-temperature magmatic system. The chalcopyrite standards were tested in several laboratories (four SIMS and one LA-ICPMS laboratories), and high homogeneity in $\delta^{34}S$ was observed. This study provides evidence that chalcopyrite samples (IGSD) are adequately homogeneous to serve as a suitable RM for in situ microanalysis. Furthermore, sufficient quantity (~ 500 g) of this material is available and laboratories around the world can request it for their use.

EXPERIMENTAL

Sample description and preparation. Chalcopyrite samples were collected from the McCreedy West deposit on the North Range of the Sudbury Igneous Complex (SIC) in Ontario, Canada (Fig. 1). SIC is a structure formed by meteorite impact at 1850 Ma.[67] It comprises three major components: (1) the main mass sequence containing quartz-earing norites, a gabbroic zone, and a granophyric zone, (2) the contact sublayer marked by small and inclusion-filled gabbronoritic bodies, and (3) the offset sublayer containing numerous dikes. The contact and offset sublayer zones are the major hosts for world-class magmatic Ni-Cu-PGE sulfide mineralization. The McCreedy West deposit is located in the western part of the Onaping-Levack Ni-Cu-PGE sulfide mineralized zone. The sulfide mineralization at the McCreedy West is massive, semi-massive, and disseminated, with sulfide assemblies of chalcopyrite, cubanite, pentlandite, pyrrhotite, and minor pyrite. Sudbury brecciated footwall contains several chalcopyrite-rich massive sulfide veins. The IGSD sample used in this study was collected from one of these veins, which is predominantly composed of almost pure chalcopyrite with a small amount of pyrrhotite or pentlandite (Fig. 2a).

The IGSD sample (~ 50 g) was crushed into small fragments. Under a microscope, chalcopyrite grains of high purity were carefully handpicked. Some chalcopyrite grains were selected and prepared for bulk analysis. Different sizes of chalcopyrite grains were cast into round epoxy mounts (diameter of 25.4 mm) with other RM (HTS4-6) (Figs. 2b and 2c). All the epoxy mounts were carefully polished several times with a diamond paste, and the grain size was gradually reduced. All the mounts were first washed in ethanol, followed by deionized water, and then heated in an oven for 3 h at 40 °C. Subsequently, several mounts were sent to SIMS and LA-MC-ICPMS laboratories to investigate the homogeneity of IGSD chalcopyrite.

Analytical techniques

EMPA. The major elemental composition was obtained using a JEOL JXA8530F-plus microprobe at the State Key Laboratory of Ore Deposit Geochemistry (SKLODG), Institution of Geochemistry, Chinese Academy of Sciences, China. The electron microprobe was equipped with five spectrometers. An acceleration voltage of 15 kV and a probe current of 20 nA with a

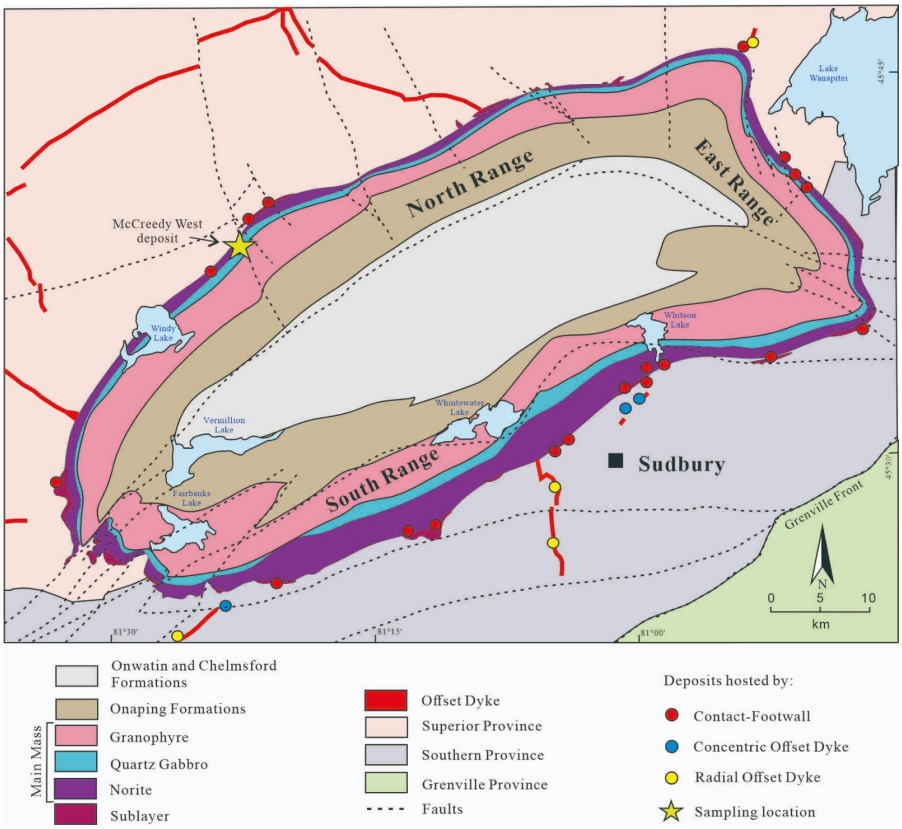

Fig. 1 Geological map of the Sudbury Igneous Complex showing the location of the McCreedy West deposit (Modified from ref. [67]).

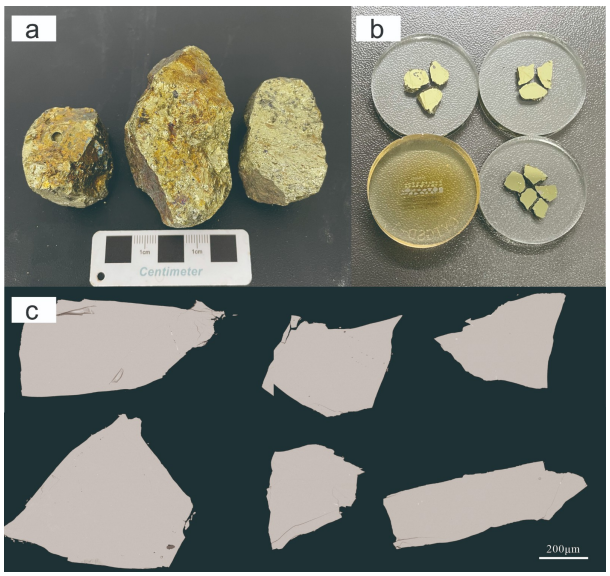

Fig. 2 (a) Photograph of IGSD chalcopyrite. (b). Mounts of different grains of IGSD chalcopyrite. (c) Typical BSE map of IGSD chalcopyrite.

beam diameter of 5 μm was applied. The following sulfides were used as standards: $CuFeS_2$ (Fe, Cu, and S), ZnS (Zn), Cd (Cd), SnO_2 (Sn), FeAsS (As), Ge (Ge), GaAs (Ga), Sb_2S_3(Sb), InP (In), PbS (S), and Ag (Ag).

IRMS. The bulk sulfur isotopic compositions ($\delta^{34}S$) of IGSD chalcopyrite were obtained using a MAT253 isotope ratio mass spectrometer coupled with an elemental analyzer (EA-IRMS) at SKLODG. The IGSD sample was crushed into several grains and sieved under a microscope to ensure high purity. The grains were then crushed to a 200-mesh using an agate mortar. The chalcopyrite (~ 180 μg) was reacted with copper wire and tungsten trioxide at 1020 °C under a vacuum pressure of 9×10^{-7} Pa, and the product SO_2 was measured using a MAT253 mass spectrometer. The analytical precision was better than 0.3 (2SD) as calculated from repeated analyses of the IAEA international standards IAEA-S-1 ($\delta^{34}S$ = –0.37‰, n = 4), IAEA-S-2 ($\delta^{34}S$ = 22.67‰, n = 5) and IAEA-S-3 ($\delta^{34}S$ = –32.49‰, n = 5).

SIMS. Four sets of SIMS measurements were performed to determine the homogeneity of the IGSD. In situ sulfur isotope analysis of IGSD chalcopyrite grains was performed using a CAMECA NanoSIMS 50 L instrument at SKLODG. The sample mounts were cleaned and then coated with a ~ 20 nm thick gold layer before analysis. A primary beam of ~ 150 pA Cs^+ with an impact energy of 16 keV was rastered on an area of 7×7 μm^2 for

150 s as the pre-sputtered time to remove the gold coating and possible contaminations, followed by a secondary ion beam (SIB) auto-centering process. Both the $^{32}S^{-}$ and $^{34}S^{-}$ ions were measured using a Faraday cup with a 1×10^{11} Ω preamplifier resistor for 300 cycles, with a cycle duration of 0.54 s each. The total analysis time, including pre-sputtering, was approximately 7 min per measurement. Other instrumental settings, including the baseline correction method, were similar to those reported by Chen *et al.*[16] Typical count rates obtained for $^{32}S^{-}$ were ~ 1.4×10^{8} cps, and the internal precision of $^{34}S/^{32}S$ for single analysis was typically 0.2‰ (2 Standard Error, 2SE). The chalcopyrite RM HTS4-6 ($\delta^{34}S$ = 0.63 ± 0.16‰,[44]) was used to correct the IMF at the beginning of the measurement. The repeatability of HTS4-6 in the test was approximately 0.3‰ (2SD, n = 10).

Another sulphur analysis was conducted at the Guangzhou Institute of Geochemistry, Chinese Academy of Sciences (GIGCAS), using a CAMECA IMS 1280-HR instrument. The analytical parameters were similar to those described by Li *et al.* [44] and are briefly summarized here. A primary Cs^{+} ion beam (~ 3.3 nA current and 20 keV total impact energy) was focused on the sample surface. The beam size was approximately 15 μm. A pre-sputtering step lasting 40 s was carried out to remove the gold coating prior to analysis. The magnetic field was stabilized during analysis using an NMR field sensor. ^{32}S and ^{34}S were simultaneously measured using two movable Faraday cups of the mutli-collector system (L1 and H'2), with resistors of 1×10^{10} Ω and 1×10^{11} Ω, respectively. The mass resolving power was set at approximately 5000 to avoid isobaric interference in the measurement. The total analysis time for each spot was approximately 4 min. Typical count rates obtained for $^{32}S^{-}$ were *ca.* 2.6×10^{9} cps, and the internal precision of $^{34}S/^{32}S$ for the analysis spot was typically 0.05‰ (2SE). The calibration reference material used for IMF correction was HTS4-6 chalcopyrite on the same mount. The repeatability of HT4-6 in the test was approximately 0.2‰ (2s, n = 8).

The homogeneity of sulfur isotopic compositions of the IGSD was tested using a CAMECA IMS 1280 SIMS at the Institute of Geology and Geophysics, Chinese Academy of Sciences (IGGCAS). The sample mounts were cleaned, and gold coated before SIMS analysis. Cesium ions were used as primary ions, and the acceleration voltage was 10 kV. The primary beam was focused in Gaussian mode with a spot of less than 10 μm in size and 360 pA in intensity. $^{32}S^{-}$ and $^{34}S^{-}$ ions were measured in multicollection using two Faraday cups with electrometers having 1×10^{10} Ω and 1×10^{12} Ω feedback resistors, respectively. The beam centering process was carried out before data acquisition. The magnification of the transfer optics was configured to approximately 133. The width of the entrance slit was 170 μm and the width of the field aperture was 4000 μm × 4000 μm. Nuclear magnetic resonance (NMR) was used to stabilize the magnetic field. Forty cycles were measured for each spot, and the integration time for each measurement cycle was 1 s. Typical count rates obtained for $^{32}S^{-}$ were ~ 5.0×10^{8} cps, and the internal precision of $^{34}S/^{32}S$ for the analysis spot was typically 0.1‰ (2SE). The homogeneity test of the IGSD was also carried out at the China University of Geosciences (CUG), Wuhan, China by using the CAMECA NanoSIMS 50 L instrument. To remove the gold coating and possible contaminations, a primary beam of 200 pA Cs^{+} with an impact energy of 16 keV was rastered on an area of 12×12 μm^2 for 120 s as the pre-sputtered time, followed by an SIB auto-centering process. Two Faraday cups with 1×10^{11} Ω preamplifier resistors were used for collecting data for 200 cycles with a cycle duration of 0.54 s each. The total analysis time, including pre-sputtering, was approximately 7 min per measurement. Typical count rates obtained for $^{32}S^{-}$ were ~ 1.7×10^{8} cps, and the internal precision of $^{34}S/^{32}S$ for single analysis was typically 0.2‰ (2SE).

LA-MC-ICPMS. In situ S isotopic analyses were conducted with a high-resolution Nu 1700 MC-ICP-MS in combination with a RESOLution S155-LR excimer ArF laser ablation system (ASI, Australia) at the State Key Laboratory of Continental Dynamics (SKLCD), Northwest University in Xi'an, China.

The laser was operated in the aperture mode with a spot size of 53 μm and a signal intensity of approximately 10 V (^{32}S signal). Argon and ultra-high He were used as auxiliary and carrier gases, respectively, and their flow rates were set at 950 and 280 mL min^{-1}, respectively. Time-resolved mode was used to determine S isotopic ratios with an integration time of 0.3 s. Each measurement lasted for 125 s, including 20 s of background measurement, 45 s of data acquisition, and 60 s of washout. The background obtained for ^{32}S was less than 200 mV. Low laser energy (3.5 J/cm^2) and laser repetition rate (3 Hz) were used to obtain a relatively stable signal intensity.

The setting of the instrument and the mass bias correction were similar to those in the reference.[43] In-house chalcopyrite (CPY-1) (chalcopyrite, $\delta^{34}S$ = 4.3 ± 0.2‰)[42] was used as the bracketing calibration for the $\delta^{34}S$ ratios. During the analysis, a reference (TC1725 chalcopyrite, $\delta^{34}S$ = 12.78 ± 0.16‰[43]) was employed to monitor IMF. The $\delta^{34}S$ value obtained from this standard (12.85 ± 0.32‰, n = 29, 2SD) was consistent with the recommended value within the margin of error.

In this study, all the measured $^{34}S/^{32}S$ ratios were normalized using Vienna-Canyon Diablo Troilite (V-CDT) standard compositions ($^{34}S/^{32}S_{V\text{-}CDT}$ = 0.0441626)[68] as $\delta^{34}S_{raw}$ (‰) = $[\{(^{34}S/^{32}S_{sample}) / (^{34}S/^{32}S_{v\text{-}CDT})\} - 1] \times 1000$. For SIMS, the IMF factor was calculated for each analysis using the relation IMF = $\delta^{34}S_{true} - \delta^{34}S_{RAW}$. Subsequently, the IMF was used to calculate the $\delta^{34}S_{cor}$ of the unknown sample using the relation $\delta^{34}S_{cor} = {}^{34}S_{RAW}$ + IMF. The $\delta^{34}S$ value was reported with the associated analytical uncertainty (SE) and standard deviation (SD), which were estimated

Table 2. EMPA data (wt %) of IGSD chalcopyrite (n = 250)

Element	Mean	2SD
Cu	34.15	0.49
Fe	30.55	0.36
S	35.47	0.34
Zn	0.05	0.05
Total	100.32	0.67

Table 3. Summary of mean values for Sulfur isotopes ($\delta^{34}S$) obtained via bulk and in situ determinations in IGSD

Method	Lab	$\delta^{34}S$ (‰)	2SD	n
EA-IRMS	SKLODG session1	4.21	0.12	9
	SKLODG session2	4.21	0.23	30
NanoSIMS	SKLODG	4.4	0.5	282
SIMS	GIGCAS	4.0	0.1	29
LA-MC-ICPMS	SKLODC session1	4.1	0.3	30
	SKLODC session2	4.3	0.2	54

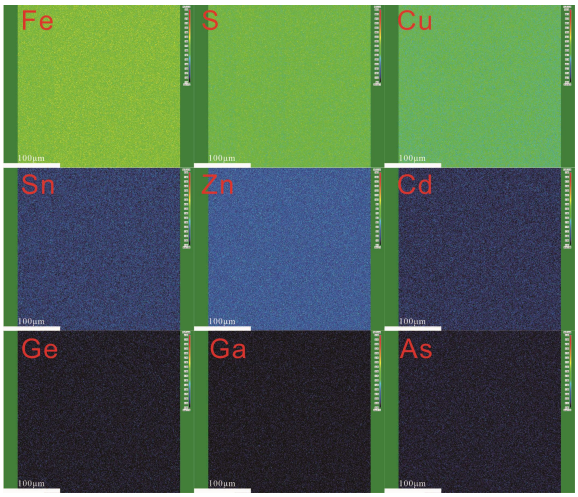

Fig. 3 Selected WDX map of IGSD chalcopyrite grains.

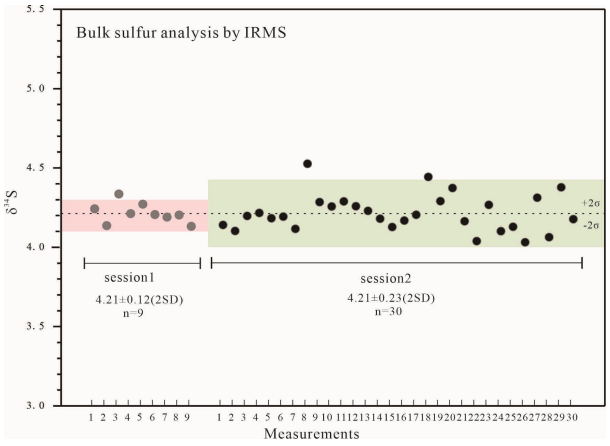

Fig. 4 Sulfur isotope compositions ($\delta^{34}S$) of IGSD chalcopyrite determined by IRMS.

as the square sum of the standard deviation of the measurement and the uncertainty of the IMF of the reference sample. The uncertainties for the RMs in the test have been propagated to the absolute $\delta^{34}S$ of the IGSD.

RESULTS AND DISCUSSION

Chemical composition of RM. To evaluate their major element characteristics and chemical homogeneity, the chemical compositions of the IGSD were measured by EMPA. The results are shown as the average values in Table 2. The detailed data of the individual measurements are listed in Supporting Information. The homogeneity of the chemical composition of IGSD chalcopyrite was assessed through the intermediate precision of the mean (2SD) of all measurements performed on the sample.

The EMPA results show that the IGSD exhibited a high degree of chemical homogeneity. The concentration of Fe varied between 29.60% and 31.64%, with an average value of 30.55% ± 0.36‰ (n=250, 2SD). Similarly, the Cu concentration ranged from 31.54% to 34.65%, with an average of 34.15% ± 0.49‰ (n = 250, 2SD). The concentration of S was found to be between 35.00% and 36.01%, with an average value of 35.47% ± 0.34‰ (n = 250, 2SD). The Zn content of the IGSD was found to be very low (< 0.14%). The concentrations of other elements (including Cd, Sn, As, Ge, Ga, Sb, Ln, Pb, and Ag) were also found to be very low, with values close to the detection limit (0.02 wt %). These results indicate that the IGSD is a highly homogeneous sample with respect to major element mass fraction. This can also be confirmed from the typical backscatter electron (BSE) map (Fig. 2c) and homogeneous wavelength dispersive X-ray (WDX) mapping with an area of 250 μm × 250 μm (Fig. 3), with no internal growth or zoning and mineral inclusions.

$\delta^{34}S$ characteristic of IGSD. The $\delta^{34}S$ value of the IGSD was determined by both bulk and in situ analyses. The summarized data of the sulfur isotopes ($\delta^{34}S$) are listed in Table 3. Detailed data can be found in Supporting Information.

$\delta^{34}S$ determined by EA-IRMS. For bulk isotope analyses, two sessions were conducted. In session 1 (November 2020), nine fragments were selected from three main parts of the IGSD (three grains each). The $\delta^{34}S$ values of the IGSD ranged from 4.14‰ to 4.34‰ (Fig. 4), yielding a mean $\delta^{34}S$ value of 4.21 ± 0.12‰ (2SD, n = 9).

In session 2 (October 2022), 15 fragments were randomly selected from three different parts of the IGSD chalcopyrite. Every sample was separated into two-subsample for $\delta^{34}S$. The $\delta^{34}S$ values of IGSD in this session ranged from 4.03‰ to 4.53‰ (Fig. 4), yielding a mean $\delta^{34}S$ value of 4.21 ± 0.23‰ (2SD, n = 30). The

bulk $\delta^{34}S$ of the IGSD in two different sessions are almost the same, confirming the reliability of the result.

$\delta^{34}S$ determined by in situ analysis. To determine the $\delta^{34}S$ value and investigate the homogeneity of the S isotopes of IGSD chalcopyrite, a total of 395 SIMS and LA-MC-ICP-MS measurements were performed on three mounts.

The $\delta^{34}S$ measurements were conducted on three large grains with crossing points in steps of 20–60 μm on NanoSIMS. A total of 282 measurements were performed with a $\delta^{34}S$ of 4.4 ± 0.5‰ (2SD) (Fig. 5a). A total of twenty-nine $\delta^{34}S$ measurements were also performed on 15 grains in GGIGCAS with a $\delta^{34}S$ of 4.0 ± 0.1‰ (2SD) (Fig. 5b).

Two sessions were carried out for the $\delta^{34}S$ measurements on three random large grains on Nu 1700 in SKLCD (Fig. 5c). During session 1 (January 2021), thirty measurements were performed with a homogeneous value of $\delta^{34}S$ = 4.1 ± 0.3‰ (2SD). However, during session 2 (January 2023), fifty-four measurements were obtained with a homogeneous value of $\delta^{34}S$ = 4.3 ± 0.2‰ (2SD).

All the $\delta^{34}S$ values determined by in situ methods are consisted within 2SD uncertainty intervals, also confirming the reliability of the result.

Homogeneity of RM. Homogeneity is a fundamental requirement for a material to qualify as an RM. Both the bulk and in situ $\delta^{34}S$ measurement at five different laboratories show that the $\delta^{34}S$ values of IGSD chalcopyrite follow a Gaussian distribution with high analysis repetition (with 2SD < 0.3‰, except for the measurements by NanoSIMS (Fig. 5). Notably, the in-situ measurement on NanoSIMS possess with lower analysis repetition (~ 0.5‰) may be due to slight detector drift during a long period (~ 35 h). This indicates that the IGSD is homogeneous in $\delta^{34}S$ characteristics.

As suggested by the key international guide for the characterization of RMs (ISO Guide 35),[69] the F-test was also conducted to examine the homogeneity of the IGSD in sulfur isotopes. The F-test for the comparison of two population variances was applied using one-way analysis of variance (ANOVA statistics). The F ratio is defined as the ratio of the between-unit variance ($S^2_{between}$) to the within-unit variance (S^2_{within}) according to the regulations of the ISO Guide 35(2017) and JJF 1343-2022.[70]

$$F=\frac{S^2_{between}}{S^2_{within}}$$

where $S^2_{between}$ is the ratio of between-unit sums of squares ($SS_{between}$) to associated degrees of freedom ($v_{between}$), and S^2_{within} is the ratio of between-unit sums of squares (SS_{within}) to associated degrees of freedom (v_{within}).

$$S^2_{between}=\frac{SS_{between}}{v_{between}}$$

$$S^2_{within}=\frac{SS_{within}}{v_{within}}$$

where $v_{between}$ and v_{within} depend on the number of units from which samples (m) are taken and the total number of replicate measurements (N), with $v_{between}$ and v_{within} calculated as follows:

$$v_{between}=\text{m-1}$$

$$v_{within}=\text{N-m}$$

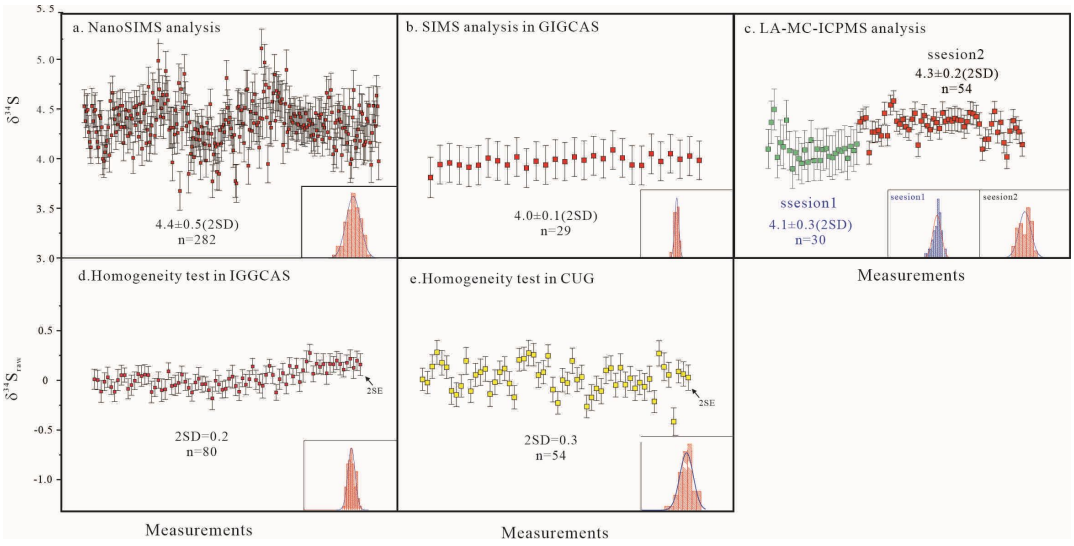

Fig. 5 Measurement and probability density curves of $\delta^{34}S$ values for IGSD in different laboratories. The range bar for a single analysis is 2SD (a,b and c). The range bar for a single analysis in homogeneity test is 2SE (d and e).

Table 4. ANOVA statistics for homogeneity testing of Sulfur isotope compositions of IGSD

	Bulk measurement with EA-IRMS	In situ measurement with NanoSIMS	In situ measurement with SIMS (GIGCAS)
m	15	3	14
N	30	282	28
$SS_{between}$	0.2191	0.1246	0.05613
SS_{within}	0.1629	14.3510	0.02694
$v_{between}$	14	2	14
v_{within}	15	279	13
F	1.44	1.21	1.93
$F_{critical}$	2.42	3.03	2.55

All ANOVA results were calculated using the Microsoft Excel software. The results are listed in Table 4.

Bulk isotope analysis. To test the homogeneity of the isotope ratios, 15 fragments of IGSD chalcopyrite were randomly selected from three large parts (Fig. 2a) (five to each). Two subsamples were then taken from each fragment, with each being treated as an independent sample. F-testing demonstrates that the bulk IRMS results of the IGSD samples have very good homogeneity at a confidence level of 95% [$F < F_{critical}$ for $\alpha = 0.05$, where α represents the sample significance level].

In situ sulfur analysis. Two F-tests of in situ analysis were performed to examine the homogeneity of IGSD in sulfur isotopes. In the first test, three large grains (5–8 mm) from different parts of the IGSD were selected and measured by NanoSIMS (SKLODG) in one session. In total, 91–96 analysis spots were distributed in a crossing pattern spaced at intervals of approximately 20–60 μm on each grain. A total of 282 measurements were performed over ~ 35 h. Each grain was treated as a sample, and the measurements on each grain were treated as replicated measurements to calculate the ANOVA statistics.

For the second test, 15 grains of the IGSD were also selected and measured by SIMS (GIGCAS). A total 28 measurements were performed by two measurements on each grain (a pair of measurements was rejected because of the bad position of one of the two measurements).

The F ratios of the samples in both of the in situ homogeneity tests were less than the $F_{critical}$ (Table 4) value of $\alpha = 0.05$, demonstrating that the in situ analyses of the IGSD samples exhibited outstanding homogeneity at a confidence level of 95%.

Therefore, both the F-test on bulk and in situ analyses demonstrated the homogeneity of IGSD chalcopyrite, indicating that IGSD chalcopyrite can be considered as a RM for in situ $\delta^{34}S$ analysis.

Recommended $\delta^{34}S$ values of IGSD. Previous homogeneous tests proved that the IGSD is homogeneous in $\delta^{34}S$. Additionally, the sulfur isotopic compositions determined at different laboratories and methods were consistent within 2SD uncertainty intervals, which were 4.4 ± 0.5‰ for NanoSIMS at SKLODG, 4.0 ± 0.1‰ for SIMS at GIGCAS, and 4.1 ± 0.3‰ and 4.3 ± 0.2‰ for LA-MC-CIPMS at SKLCD. These values were also consistent with the result of the bulk sulfur isotope analysis (4.21 ± 0.12‰ in session 1 and 4.21 ± 0.23‰ in session 2), confirming the accuracy of sulfur isotopic compositions. Therefore, the $\delta^{34}S$ value of 4.21 ± 0.23‰ (2SD, n = 30) of IRMS is the recommended value for IGSD chalcopyrite.

CONCLUSION

This study demonstrated that the IGSD chalcopyrite sample is homogeneous with respect to major element and $\delta^{34}S$ compositions. This sulfide mineral is suitable as an RMs for S isotope microanalysis through SIMS and LA-MC-ICPMS. The best recommended value of $\delta^{34}S$ is 4.21 ± 0.23‰ (2SD) of IRMS for IGSD chalcopyrite.

Currently, approximately 500 g of the IGSD grains is stored in the NanoSIMS laboratory at SKLODG and is available for distribution. Interested parties may request access to the material from the first author of this article.

ASSOCIATED CONTENT

The supporting information (Detailed data) is available at www.at-spectrose.com/as/home.

AUTHOR INFORMATION

Youwei Chen received B.S. degree in geochemistry from Nanjing university in 2005 and Ph.D. degree in geochemistry of ore deposit from institution of geochemistry, Chinese Academy of Sciences (IGCAS) in 2010. He is an associate professor of geochemistry at the IGCAS and currently in charge of the NanoSIMS laboratory. His interest on microanalysis was initiated since 2017 at LA-

MC-ICPMS. Then he started working on NanoSIMS in 2020. His major research interests are SIMS methods development, NanoSIMS application on ore deposit, and the formation of the uranium deposit, *etc*.

Jianfeng Gao received his BSc in 1999 and MSc in 2005 from Nanjing University, and PhD in 2013 from the University of Hong Kong. He is a research professor of geochemistry at the Institute of Geochemistry, Chinese Academy of Sciences. His major research interests are analytical techniques of elemental and isotopic analysis and their applications to igneous petrogenesis, and magmatic-hydrothermal mineralization systems. He has been working as member of editorial board for *Atomic Spectroscopy*.

Corresponding Author

* Y. W. Chen

Email address: chenyouwei@mail.gyig.ac.cn

* J. F. Gao

Email address: gaojianfeng@mail.gyig.ac.cn

Notes

The authors declare no competing financial interest.

ACKNOWLEDGMENTS

We thank Dr. Qiuli Li and Dr. Xiaoping Xia for their help in in situ sulfur isotope analysis, and Axel Schmitt from Curtin university for his thoughtful comments to an earlier version of this manuscript. We also thank the editor and three anonymous reviewers for their insightful and detailed comments, which significantly enhanced the manuscript. This research was jointly supported by the National Key Research and Development Program of China (2018YFA0702602) and the National Natural Science Foundation of China (42025301).

REFERENCES

1. H. Ohmoto, *Geochemistry of hydrothermal ore deposits*, 1979, 509–567. https://cir.nii.ac.jp/crid/1573105975177859072
2. N. V. Grassineau, D. P. Mattey, and D. Lowry, *Anal. Chem.*, 2001, **73**, 220–225. https://doi.org/10.1021/ac000550f
3. D. E. Canfield, *Am. J. Sci.*, 2004, **304**, 839–861. https://doi.org/10.2475/ajs.304.10.839
4. W. C. Shanks III, *Rev. Mineral. Geochem.*, 2001, **43**, 469–525. https://doi.org/10.2138/gsrmg.43.1.469
5. P. R. Mason, J. Košler, J. C. De Hoog, P. J. Sylvester, and S. Meffan-Main, *J. Anal. At. Spectrom.*, 2006, **21**, 177–186. https://doi.org/10.1039/B510883G
6. B. Rottier, and A. Audétat, *Chem. Geol.*, 2019, **504**, 1–13. https://doi.org/10.1016/j.chemgeo.2018.11.012
7. J. De Hoog, P. Mason, and M. van Bergen, *Geochim. Cosmochim. Acta*, 2001, **65**, 3147–3164. https://doi.org/10.1016/S0016-7037(01)00634-2
8. Z. A. Bao, L. Chen, C. L. Zong, H. L. Yuan, K. Y. Chen, and M. L. Dai, *Int. J. Mass Spectrom.*, 2017, **421**, 255–262. https://doi.org/10.1016/j.ijms.2017.07.015
9. L. R. Riciputi, B. A. Paterson, and R. L. Ripperdan, *Int. J. Mass Spectrom.*, 1998, **178**, 81–112. https://doi.org/10.1016/S1387-3806(98)14088-5
10. J. Hammerli, N. D. Greber, L. Martin, A.-S. Bouvier, A. I. Kemp, M. L. Fiorentini, J. E. Spangenberg, Y. Ueno, and U. Schaltegger, *Chem. Geol.*, 2021, **579**, 120242. https://doi.org/10.1016/j.chemgeo.2021.120242
11. E. H. Hauri, D. Papineau, J. H. Wang, and F. Hillion, *Chem. Geol.*, 2016, **420**, 148–161. https://doi.org/10.1016/j.chemgeo.2015.11.013
12. R. Kozdon, N. T. Kita, J. M. Huberty, J. H. Fournelle, C. A. Johnson, and J. W. Valley, *Chem. Geol.*, 2010, **275**, 243–253. https://doi.org/10.1016/j.chemgeo.2010.05.015
13. N. T. Kita, J. M. Huberty, R. Kozdon, B. L. Beard, and J. W. Valley, *Surf. Interface Anal.*, 2011, **43**, 427–431. https://doi.org/10.1002/sia.3424
14. C. LaFlamme, L. Martin, H. Jeon, S. M. Reddy, V. Selvaraja, S. Caruso, T. H. Bui, M. P. Roberts, F. Voute, S. Hagemann, D. Wacey, S. Littman, B. Wing, M. Fiorentini, and M. R. Kilburn, *Chem. Geol.*, 2016, **444**, 1–15. https://doi.org/10.1016/j.chemgeo.2016.09.032
15. M. Pimminger, M. Grasserbauer, E. Schroll, and I. Cerny, *Anal. Chem.*, 1984, **56**, 407–411. https://doi.org/10.1021/ac00267a024
16. W. Y. Chen, Z. J. Xie, S. H. Dong, Q. L. Lei, and J. F. Gao, *J. Anal. At. Spectrom.*, 2022, **37**, 2529–2536. https://doi.org/10.1039/D2JA00248E
17. J. C. Zhang, Y. T. Lin, W. Yang, W. J. Shen, J. L. Hao, S. Hu, and M. J. Cao, *J. Anal. At. Spectrom*., 2014, **29**, 1934–1943. https://doi.org/10.1039/c4ja00140k
18. R. Economos, P. Boehnke, and A. Burgisser, *Geochim. Cosmochim. Acta*, 2017, **215**, 387–403. https://doi.org/10.1016/j.gca.2017.08.015
19. Y. F. Wu, K. Evans, S. Y. Hu, D. Fougerouse, M. F. Zhou, L. A. Fisher, P. Guagliardo, and J. W. Li, *Geology*, 2021, **49**, 827–831. https://doi.org/10.1130/g48443.1
20. T. Ushikubo, K. H. Williford, J. Farquhar, D. T. Johnston, M. J. Van Kranendonk, and J. W. Valley, *Chem. Geol.*, 2014, **383**, 86–99. https://doi.org/10.1016/j.chemgeo.2014.06.006
21. S. Xiao, J. D. Schiffbauer, K. A. McFadden, and J. Hunter, *Earth Planal Sci. Lett.*, 2010, **297**, 481–495. https://doi.org/10.1016/j.epsl.2010.07.001
22. M. L. Gomes, D. A. Fike, K. D. Bergmann, C. Jones, and A. H. Knoll, *Geobiology*, 2018, **16**, 17–34. https://doi.org/10.1111/gbi.12265
23. J. Hammerli, A. I. S. Kemp, N. Barrett, B. A. Wing, M. Roberts, R. J. Arculus, P. Boivin, P. M. Nude, and K. Rankenburg, *Chem. Geol.*, 2017, **454**, 54–66. https://doi.org/10.1016/j.chemgeo.2017.02.016
24. N. T. Kita, T. Ushikubo, B. Fu, and J. W. Valley, *Chem. Geol.*, 2009, **264**, 43–57. https://doi.org/10.1016/j.chemgeo.2009.02.012
25. G. Othmane, S. Hull, M. Fayek, O. Rouxel, M. Lahd Geagea, and T. K. Kyser, *Chem. Geol.*, 2015, **395**, 41–49.

https://doi.org/10.1016/j.chemgeo.2014.11.024

26. J. M. Eiler, C. Graham, and J. W. Valley, *Chem. Geol.,* 1997, **138**, 221–244. https://doi.org/10.1016/S0009-2541(97)00015-6
27. M. J. Whitehouse, *Geostand. Geoanal. Res.*, 2013, **37**, 19–33. https://doi.org/10.1111/j.1751-908X.2012.00188.x
28. E. Dubinina, A. Borisov, M. Wiedenbeck, and A. Rocholl, *Chem. Geol.*, 2021, **578**, 120322. https://doi.org/10.1016/j.chemgeo.2021.120322
29. R. A. Cabral, M. G. Jackson, E. F. Rose-Koga, K. T. Koga, M. J. Whitehouse, M. A. Antonelli, J. Farquhar, J. M. D. Day, and E. H. Hauri, *Nature*, 2013, **496**, 490–493. https://doi.org/10.1038/nature12020
30. J. M. Huberty, N. T. Kita, R. Kozdon, P. R. Heck, J. H. Fournelle, M. J. Spicuzza, H. F. Xu, and J. W. Valley, *Chem. Geol.*, 2010, **276**, 269–283. https://doi.org/10.1016/j.chemgeo.2010.06.012
31. K. Y. Chen, Z. A. Bao, P. Liang, X. J. Nie, C. L. Zong, and H. L. Yuan, *Spectrochim. Acta, Part B*, 2022, **188**, 106344. https://doi.org/10.1016/j.sab.2021.106344
32. P. R. Craddock, O. J. Rouxel, L. A. Ball, and W. Bach, *Chem. Geol.*, 2008, **253**, 102–113. https://doi.org/10.1016/j.chemgeo.2008.04.017
33. S. E. Gilbert, L. V. Danyushevsky, T. Rodemann, N. Shimizu, A. Gurenko, S. Meffre, H. Thomas, R. R. Large, and D. Death, *J. Anal. At. Spectrom.*, 2014, **29**, 1042–1051. https://doi.org/10.1039/C4JA00011K.
34. F. Molnár, I. Mänttäri, H. O'Brien, Y. Lahaye, L. Pakkanen, B. Johanson, A. Käpyaho, P. Sorjonen-Ward, M. Whitehouse, and G. Sakellaris, *Ore Geol. Rev.*, 2016, **77**, 133–162. https://doi.org/10.1016/j.oregeorev.2016.02.012
35. Y. T. Feng, W. Zhang, Z. C. Hu, Y. S. Liu, K. Chen, J. L. Fu, J. Y. Xie, and Q. H. Shi, *J. Anal. At. Spectrom.*, 2018, **33**, 2172–2183. https://doi.org/10.1039/C8JA00305J
36. Y. T. Feng, W. Zhang, Z. C. Hu, T. Luo, M. Li, Y. S. Liu, H. Liu, and Q. L. Li, *J. Anal. At. Spectrom.*, 2022, **37**, 551–562. https://doi.org/10.1039/d1ja00392e
37. N. Lv, Z. A. Bao, K. Y. Chen, C. L. Zong, Y. Zhang, and H. L. Yuan, *Geostand. Geoanal. Res.*, 2022, **46**, 451–463. https://doi.org/10.1111/ggr.12440
38. D. E. Crowe, and R. G. Vaughan, *Am. Mineral.*, 1996, **81**, 187–193. https://doi.org/10.2138/am-1996-1-223
39. S. J. Mojzsis, C. D. Coath, J. P. Greenwood, K. D. McKeegan, and T. M. Harrison, *Geochim. Cosmochim. Acta*, 2003, **67**, 1635–1658. https://doi.org/10.1016/S0016-7037(03)00059-0
40. Y. Kitayama, E. Thomassot, J. O'Neil, and B. A. Wing, *Earth Planet. Sci. Lett.*, 2012, **15**, 355-356. 271–282. https://doi.org/10.1016/j.epsl.2012.08.026
41. J. Farquhar, J. Cliff, A. L. Zerkle, A. Kamyshny, S. W. Poulton, M. Claire, D. Adams, and B. Harms, *Proc. Natl. Acad. Sci.*, 2013, **110**, 17638–17643. https://doi.org/10.1073/pnas.1218851110
42. L. Chen, K. Y. Chen, Z. A. Bao, P. Liang, T. T. Sun, and H. L. Yuan, *J. Anal. At. Spectrom.*, 2017, **32**, 107–116. https://doi.org/10.1039/C6JA00270F
43. Z. A. Bao, K. Y. Chen, C. L. Zong, and H. L. Yuan, *J. Anal. At. Spectrom.,* 2021, **36**, 1657–1665. https://doi.org/10.1039/d1ja00168j
44. R. C. Li, X. P. Xia, H. Y. Chen, N. P. Wu, T. P. Zhao, C. Lai, Q. Yang, and Y. Q. Zhang, *Geostand. Geoanal. Res.,* 2020, **44**, 485–500. https://doi.org/10.1111/ggr.12330
45. M. J. Pribil, W. I. Ridley, and P. Emsbo, *Chem. Geol.*, 2015, **412,** 99–106. https://doi.org/10.1016/j.chemgeo.2015.07.014
46. X. J. Nie, Z. A. Bao, C. L. Zong, N. Lv, K. Y. Chen, and H. L. Yuan, *J. Anal. At. Spectrom.*, 2023, **38**, 1065–1075. https://doi.org/10.1039/D2JA00394E
47. L. Chen, H. L. Yuan, K. Y. Chen, Z. A. Bao, L. M. Zhu, and P. Liang, *J. Asian Earth Sci.*, 2019, **176**, 325–336. https://doi.org/10.1016/j.jseaes.2019.02.017
48. R. C. Li, X. P. Xia, S. H. Yang, H. Y. Chen, and Q. Yang, *Geostand. Geoanal. Res.*, 2018, **43**, 177–187. https://doi.org/10.1111/ggr.12244
49. L. Chen, Y. Liu, Y. Li, Q. L. Li, and X.-H. Li, *J. Anal. At. Spectrom.*, 2021, **36**, 1431–1440. https://doi.org/10.1039/d1ja00029b
50. G. Q. Xie, J. W. Mao, W. Li, B. Fu, and Z. Y. Zhang, *Miner. Deposita*, 2019, **54,** 67–80. https://doi.org/10.1007/s00126-018-0805-5
51. S.-J. Barnes and P. C. Lightfoot, *Economic Geology One Hundredth Anniversary Volumem*, GeoScienceWorld, 2005. https://doi.org/10.5382/AV100.08
52. R. H. Sillitoe, *Econ. Geol.*, 2010, **105**, 3–41. https://doi.org/10.2113/gsecongeo.105.1.3
53. M. D. Barton, *Treatise on Geochemistry (Second Edition)*, 2014, **13**, 515–541. https://doi.org/10.1016/B978-0-08-095975-7.01123-2
54. D. I. Groves, F. P. Bierlein, L. D. Meinert, and M. W. Hitzman, *Econ. Geol.,* 2010, **105**, 641–654. https://doi.org/10.2113/gsecongeo.105.3.641
55. A. E. Williams-Jones and C. A. Heinrich, *Econ. Geol.*, 2005, **100**, 1287–1312. https://doi.org/10.2113/gsecongeo.100.7.1287
56. M. W. Hitzman, D. Selley, and S. Bull, *Econ. Geol.*, 2010, **105,** 627–639. https://doi.org/10.2113/gsecongeo.105.3.627
57. D. C. Harris, L. J. Cabri, and R. Nobiling, *Can. Mineral.*, 1984, **22**, 493–498. https://pubs.geoscienceworld.org/canmin/article-abstract/22/3/493/11747/Silver-bearing-chalcopyrite-a-principal-source-of
58. J. M. McDermott, S. Ono, M. K. Tivey, J. S. Seewald, W. C. Shanks, and A. R. Solow, *Geochim. Cosmochim. Acta*, 2015, **160**, 169–187. https://doi.org/10.1016/j.gca.2015.02.016
59. M. Reich, N. Román, F. Barra, and D. Morata, *Minerals,* 2020, **10,** 113. https://doi.org/10.3390/min10020113
60. K. A. Evans, A. G. Tomkins, J. Cliff, and M. L. Fiorentini, *Chem. Geol.*, 2014, **365**, 1–19. https://doi.org/10.1016/j.chemgeo.2013.11.026
61. F. Giacometti, K. A. Evans, G. Rebay, J. Cliff, A. G. Tomkins, P. Rossetti, G. Vaggelli, and D. T. Adams, *Geochem., Geophys., Geosyst.*, 2014, **15**, 3808-3829. https://doi.org/10.1002/2014GC005459
62. K. K. Sun, B. Chen, J. Deng, and X. H. Ma, *Ore Geol. Rev.*, 2018, **101**, 919–935. https://doi.org/10.1016/j.oregeorev.2018.08.029
63. P. Liang, L. Chen, R. C. Li, Y.L. Xie, C. Wu, and C.-K. Lai, *Ore Geol. Rev.*, 2021, **139**, 104510. https://doi.org/10.1016/j.oregeorev.2021.104510
64. D. M. Tang, K. Z. Qin, B. X. Su, Y. J. Mao, N. J. Evans, Y. J. Niu, and Z. Kang, *Geochim. Cosmochim. Acta*, 2020, **275**, 209–228. https://doi.org/10.1016/j.gca.2020.02.015
65. K. L. Shelton and D. M. Rye, *Econ. Geol.*, 1982, **77**, 1688–1709. https://doi.org/10.2113/gsecongeo.77.7.1688
66. P. M. Herzig, M. D. Hannington, and A. Arribas Jr, *Miner. Deposita*, 1998, **33**, 226–237. https://doi.org/10.1007/s001260050143
67. P. C. Lightfoot, *Nickel sulfide ores and impact melts: Origin of the Sudbury Igneous Complex*, Elsevier, 2017.

https://doi.org/10.1016/B978-0-12-804050-8.00002-X

68. T. Ding, S. Valkiers, H. Kipphardt, P. De Bièvre, P. D. P. Taylor, R. Gonfiantini, and R. Krouse, *Geochim. Cosmochim. Acta*, 2001, **65**, 2433–2437. https://doi.org/10.1016/S0016-7037(01)00611-1
69. ISO Guide 35, International Organization for Standardization (Geneva), 2017. https://www.iso.org/standard/60281.html
70. State Administration for Market Regulation of the People's Republic of China. Standards Press of China: Beijing, 2022, p76. http://jjg.spc.org.cn/resmea/standard/JJF%25201343-2022/?